Mapping Local Protein Electrostatics by EPR of pH-Sensitive Thiol-Specific Nitroxide[†,‡]

Maxim A. Voinov,[§] Andres Ruuge,[§] Vladimir A. Reznikov,[||] Igor A. Grigor'ev,[||] and Alex I. Smirnov*[,§]

Department of Chemistry, North Carolina State University, 2620 Yarbrough Drive, Raleigh, North Carolina 27695, and Novosibirsk Institute of Organic Chemistry, Akad. Lavrent'ev Ave. 9, Novosibirsk 630090, Russia

Received February 15, 2008; Revised Manuscript Received March 27, 2008

ABSTRACT: A first thiol-specific pH-sensitive nitroxide spin-label of the imidazolidine series, methanethiosulfonic acid *S*-(1-oxyl-2,2,3,5,5-pentamethylimidazolidin-4-ylmethyl) ester (IMTSL), has been synthesized and characterized. X-Band (9 GHz) and W-band (94 GHz) EPR spectral parameters of the new spin-label in its free form and covalently attached to an amino acid cysteine and a tripeptide glutathione were studied as a function of pH and solvent polarity. The pK_a value of the protonatable tertiary amino group of the spin-label was found to be unaffected by other ionizable groups present in side chains of unstructured small peptides. The W-band EPR spectra were shown to allow for pK_a determination from precise *g*-factor measurements. Is has been demonstrated that the high accuracy of pK_a determination for pH-sensitive nitroxides could be achieved regardless of the frequency of measurements or the regime of spin exchange: fast at X-band and slow at W-band. IMTSL was found to react specifically with a model protein, iso-1-cytochrome *c* from the yeast *Saccharomyces cerevisiae*, giving EPR spectra very similar to those of the most commonly employed cysteine-specific label MTSL. CD data indicated no perturbations to the overall protein structure upon IMTSL labeling. It was found that for IMTSL, g_{iso} correlates linearly with A_{iso}, but the slopes are different for the neutral and charged forms of the nitroxide. This finding was attributed to the solvent effects on the spin density at the oxygen atom of the NO group and on the excitation energy of the oxygen lone-pair orbital.

Electrostatic interactions and hydrogen bonding play fundamental roles in virtually all aspects of protein structure and function. Solvent polarity and the presence of localized charges affect protein stability and protein−protein interactions and modulate the binding and insertion of proteins and peptides into lipid bilayers (*1, 2*). While basics of solvation effects for molecules are well understood, applications of the same principles to proteins and lipid−protein complexes are less straightforward because of the large number of interactions involved. Indeed, explicit molecular-level treatment of protein solvation processes requires detailed evaluations and averaging of electrostatic and van der Waals energy terms over a large number of solvent molecules and protein side chain configurations. One very useful approach for predicting electrostatic properties of large molecular assemblies is based on treating the solvent as a dielectric continuum and solving the classical Poisson−Boltzmann equation (PBE)[1] digitally for realistic molecular surfaces (*3*). This classical electrostatic model is then combined with computationally efficient algorithms for solving PBE for complex shapes and charge distributions on a finite grid. Such an approach has proven to be successful in modeling solvent- and pH-dependent protein phenomena with at least semiquantitative accuracy (*3, 4*). Recently, some more progress in modeling of electrostatic properties has been achieved by developing methods that include polarizable force fields (*5*) and/or generalized Born and other techniques for molecular dynamics simulations of proteins and RNA with a continuum solvent (*6*). One important conclusion of a recent theoretical study of four different proteins under various conditions of pH, temperature, solvation, or ligand binding was that behavior of the charged residues is the primary determinant of the protein effective static dielectric permittivity, $\epsilon(0)$ (*7*). Furthermore, only environmental changes that altered the properties of charged residues were found to exert a significant effect on $\epsilon(0)$. In contrast, buried water molecules

[†] This work was initiated by NATO Collaborative Linkage Grant LST.CLG.977528. The work of the Novosibirsk group is also supported by the Russian Foundation for Basic Research (RFBR), Grant 01-03-32452a. The work of the North Carolina State University laboratory in Raleigh is supported by the U.S. Department of Energy (Contract W-31-109-Eng-38), the National Science Foundation (NSF ECS 0420775), and the National Institutes of Health (1R01GM072897). M.A.V. is thankful for the NSF-NATO fellowship (DGE-0312165) for generous support.

[‡] Preliminary communication published (*29*).

* To whom correspondence should be addressed. Telephone: (919) 513-4377. Fax: (919) 513-7353. E-mail: Alex_Smirnov@ncsu.edu.

[§] North Carolina State University.

[||] Novosibirsk Institute of Organic Chemistry.

[1] Abbreviations: EPR, electron paramagnetic resonance; IMTSL, methanethiosulfonic acid *S*-(1-oxyl-2,2,3,5,5-pentamethylimidazolidin-4-ylmethyl) ester; MTSL, methanethiosulfonic acid S-(1-oxyl-2,2,5,5-tetramethylpyrroline-3-ylmethyl) ester; CD, circular dichroism; PBE, Poisson−Boltzmann equation; THEMATICS, theoretical microscopic titration curves; NMR, nuclear magnetic resonance; HF EPR, high-field electron paramagnetic resonance; SDSL, site-directed spin labeling; MTS, methanethiosulfonate; HPLC, high-performance liquid chromatography; far-UV, far ultraviolet; PTFE, polytetrafluoroethylene; PDT, 4-oxo-2,2,6,6-tetramethylpiperidine-d_{16} 1-oxyl; CP, 3-carboxy-2,2,5,5-tetramethylpyrrolidine 1-oxyl; RH3, 2,2,3,4,5,5-hexamethylimidazolidine 1-oxyl.

10.1021/bi800272f CCC: $40.75
Published on Web 04/22/2008

or ligands have little or no effect on proteins (*7*). Thus, it appears that the charged surface side chains play the primary role in determining the electrostatic properties of proteins. Furthermore, there is accumulating evidence that protein side chains exhibiting perturbed electrostatic behavior tend to occur in enzymes' active sites with sufficient frequency and, therefore, could serve as useful markers of chemical reactivity (*8*). Such sites could be identified, for example, by a THEMATICS (theoretical microscopic titration curves) method that is based on Poisson−Boltzmann calculations of the electrical potential function of a protein structure, followed by a Monte Carlo procedure for computing the mean net charge for each of the ionizable sites as a function of pH (*8–10*). As the theoretical models evolve to become more detailed and complete, the onus is shifting to the development of experimental methods that are capable of providing quantitative data for a critical comparison (*11*).

From an experimental point of view, local electrostatic interactions remain somewhat elusive parameters because of the scarcity of the experimental methods capable of measuring these effects accurately and unambiguously. One of the most powerful methods of structural biology, high-resolution NMR, can be utilized directly or indirectly to access complex electrostatics of biomolecules. Residue-specific pK_a values can be determined directly by NMR of protein and RNA samples that are labeled with ^{13}C and ^{15}N isotopes uniformly (*12*) or selectively (*13*). Special NMR pulse sequences have been developed to measure the ^{13}C chemical shifts even for unfolded protein states where the chemical shift overlap is limiting (*12*). However, for the unambiguous determination of pK_a values, the dynamics of proton exchange has to be slow on the NMR time scale. NMR can also be used to access the electrostatic potential distribution around proteins and other molecules by measuring site-specific proton relaxation enhancement upon collisions of exposed residues with nitroxide spin probes bearing different electrical charges (*14*). This relaxation enhancement depends upon the collision frequency of a particular side chain proton with a charged nitroxide molecule and, therefore, is affected by a local electric field. While this NMR nitroxide accessibility method yields surface potentials that are in a good agreement with theoretically predicted values, it is applicable only to proteins with resolved and assigned NMR spectra. This complicates the adaptation of this NMR method to large membrane proteins.

To address some of the shortcomings of the existing experimental techniques, Cohen et al. (*15*) utilized a labeling approach that is based on an unnatural amino acid Aladan, which can be specifically incorporated into a protein by nonsense suppression and reports on the electrostatic character of a protein by steady-state and time-resolved fluorescence.

Another labeling method that could be used to probe local electric fields and hydrogen bonding interactions is based on EPR of stable nitroxide radicals. Magnetic parameters of nitroxides are known to be sensitive to intermolecular interactions and, in particular, to hydrogen bonding and local solvent polarity (*16–18*). In general, when a spin-labeled molecule is transferred from an aqueous (polar) to a hydrocarbon (nonpolar) environment, the isotropic nitrogen hyperfine constant A_{iso} decreases by up to ~2 G while the isotropic g factor, g_{iso}, increases by ~0.0004. At X-band (9 GHz) Larmor frequency, this change in g_{iso} corresponds to an ~0.68 G shift of the EPR line that is smaller than the typical nitroxide line width (~1 G). However, this spectral shift can be amplified by carrying out EPR experiments at high magnetic fields (HF EPR). For example, at W-band (ca. 95 GHz, corresponding magnetic field of 34000 G for $g = 2$), the shift in the positions of the resonance lines due to the g-factor differences is magnified 10-fold to ~6.8 G, thus exceeding the corresponding changes in A_{iso}.

In the past, magnetic parameters (both **g** matrices and **A** tensors) determined with high accuracy from the rigid limit EPR spectra at high magnetic fields have been utilized to characterize nitroxide−solvent interactions and solvent polarity (*18*). More recent applications are exemplified by HF EPR studies of a polarity profile along the lipid binding channel of Sec14p protein using a series of doxyl-labeled stearic acids (*19, 20*) and an examination of spin-labeled side chains of a membrane protein bacteriorhodopsin (*21, 22*). The latter studies employed a site-directed spin labeling (SDSL) method. Briefly, in application to proteins, SDSL involves site-directed cysteine substitution mutagenesis at desirable sites of the protein sequence (*23*). Then thiol-specific reagents, such as methanethiosulfonate (MTS), maleimide derivatives, or others, are utilized to covalently attach a nitroxide label to a cysteine SH group. The MTS attachment group has a clear advantage over the maleimide because of the high specificity to the sulfhydryl group of proteins (*24*). Although, in principle, several different nitroxide labels can be linked to the protein sulfhydryl groups using MTS chemistry, almost all SDSL EPR studies up to date have been carried out with methanethiosulfonate spin-label MTSL, methanethiosulfonic acid S-(1-oxyl-2,2,5,5-tetramethylpyrroline-3-ylmethyl) ester. This label is rather small and, when attached to a cysteine, causes little or negligible perturbations to the protein structure and function (*25*).

While MTSL has been proven to be a very useful nitroxide for SDSL EPR protein studies, the arsenal of EPR experiments could be further expanded via the development of new free radical-bearing molecular probes with additional reporting capabilities. In particular, pH-sensitive nitroxide labels could be very useful for probing the complex landscape of protein electrostatics. Among nitroxides, imidazoline and imidazolidine derivatives containing protonatable functionalities within the structure of a heterocycle are considered to be the most promising for biophysical applications because of (i) the high sensitivity of the EPR spectrum to pH changes, (ii) the tunable pK_a range, and (iii) the reversibility of the pH effect (*26*). These properties have been utilized by Khramtsov and co-workers to evaluate the surface potentials and polarity of phospholipid bilayers (*27*) and human serum albumin (*28*), although the nitroxide covalent attachment was not fully specific.

Here we describe a general approach for mapping local pK_a values of protein side chains with spin labeling EPR. We show that accurate g-factor determination achieved at high magnetic fields provides some new information about electric field effects and allows for differentiation between polarity and pH effects on EPR spectra of the imidazolidine nitroxide in a single experiment. We characterize a new thiol-specific pH-sensitive nitroxide−methanethiosulfonate derivative of an imidazolidine nitroxide [methanethiosulfonic acid *S*-(1-oxyl-2,2,3,5,5-pentamethylimidazolidin-4-ylmethyl) es-

ter (IMTSL)] (see ref *29*). We demonstrate that IMTSL reacts specifically with a unique cysteine of a model protein, iso-1-cytochrome *c* from the yeast *Saccharomyces cerevisiae*, giving rise to EPR spectra that are very similar to those of MTSL. We also report on EPR spectral parameters of the new nitroxide label in its free form and upon attachment to the free amino acid cysteine and a tripeptide glutathione as a function of the pH and polarity of solvents. Finally, we report on the use of this new pH-sensitive spin-label to study local pK_a values in a peptide P11, which consists of residues 925−933 of the B1 chain of the basement membrane-specific glycoprotein laminin.

MATERIALS AND METHODS

Materials. All chemicals were purchased from Sigma-Aldrich (St. Louis, MO) or Acros Organics (Morris Planes, NJ) unless otherwise indicated. All solvents were reagent grade and used as received. Synthesis of the thiol-specific pH-sensitive spin-label IMTSL was described in our preliminary communication (*29*).

Two other nitroxides utilized in this study include perdeuterated Tempone (4-oxo-2,2,6,6-tetramethylpiperidine-d_{16} 1-oxyl, or PDT, purchased from Cambridge Isotope Laboratories, Andover, MA) and 3-carboxy-2,2,5,5-tetramethylpyrrolidine 1-oxyl (CP, purchased from Sigma-Aldrich). These nitroxides were used as received for preparation of 10 mM stock solutions in deionized water.

EPR titration experiments were carried out with the following set of standard buffer solutions purchased from VWR International (West Chester, PA): (a) potassium tetraoxalate at pH 1.68, (b) hydrochloric acid/glycine at pH 2.0, (c) potassium hydrogen phthalate/hydrochloric acid at pH 3.0, (d) potassium hydrogen phthalate at pH 4.0, e) acetic acid/sodium acetate at pH 4.63, (f) potassium hydrogen phthalate/sodium hydroxide at pH 5.0, (g) potassium hydrogen phthalate/sodium hydroxide at pH 6.0, (h) sodium phosphate/potassium phosphate at pH 6.86, 7.0, 7.38, and 8.0, (i) boric acid/potassium chloride/sodium hydroxide at pH 9.0, (j) sodium borate at pH 9.18, and (k) sodium bicarbonate/sodium carbonate at pH 10. All buffer solutions contained 0.5% biocide Dowicide A (sodium *o*-phenylphenate tetrahydrate) and were at a concentration of 50 mM, except the phosphate buffer (pH 6.86) which was at a concentration of 25 mM. These reference buffer solutions are specified to be accurate to at least ±0.02 pH unit at 25 °C and deviate from the specified values by not more than ±0.05 pH unit at 40 °C. Some measurements were carried out with freshly prepared potassium hydrogen phthalate/hydrochloric acid buffers. In addition, a 0.1 N solution of HCl at pH 1.1 (*30*) was used.

A fragment of the laminin B1 chain Cys-Asp-Pro-Gly-Tyr-Ile-Gly-Ser-Arg (P11 peptide) was synthesized by SynPep (Dublin, CA) and specified to be 95.3% pure by HPLC.

Labeling of Proteins and Peptides. Typically, an 80 mM IMTSL stock solution was prepared in 0.5 mL of dry DMSO. The solution was kept under an airtight seal in a −20 °C freezer. Fresh 100 mM solutions of glutathione or L-cysteine were prepared in distilled water. Labeling of the thiols was carried out by adding an IMTSL stock to an at least 2-fold excess of glutathione or L-cysteine solutions. These reactions were allowed to proceed at room temperature for ≥40 min. The resulting mixtures were used without further purification. To verify the absence of unreacted IMTSL, labeling experiments with 5- and 10-fold excesses of amino acids were also carried out. No changes in EPR spectra were observed under these conditions.

Labeling of the P11 Peptide. For labeling of the fragment of the laminin B1 chain, a 50 mM peptide solution in distilled water was freshly prepared and mixed with a 3-fold excess of IMTSL from a DMSO stock. The reaction was allowed to proceed for 1.5 h at room temperature. The products were separated by a reverse-phase HPLC system (Varian C_{18} column, Varian, Walnut Creek, CA) using acetonitrile in 0.1% aqueous trifluoroacetic acid (linear gradient from 15 to 40%). After the separation, the samples were immediately lyophilized and stored in a −20 °C freezer.

Labeling of Iso-1-cytochrome c. Labeling of the iso-1-Cytochrome *c* Cys 102 residue was carried out for 1.5 h at room temperature by mixing a 100 mM protein solution in a 10 mM MOPS buffer (pH 6.6) with an at least 2-fold excess of IMTSL. The mixture was vortexed occasionally. Unreacted spin-label was removed using Sephadex G 25 M disposable columns (Amersham Biosciences, Piscataway, NJ). Purified protein was further concentrated using a Microcon YM-30 centrifugal filter device (Millipore Corp., Billerica, MA). CD spectra of spin-labeled iso-1-cytochrome *c* were recorded at room temperature with a Jasco J-720 spectropolarimeter installed at the Laboratory for Fluorescence Dynamics (University of Illinois, Urbana, IL) and compared with those of unlabeled protein. pH-induced denaturation of IMTSL-labeled iso-1-cytochrome *c* was monitored by the far-UV CD signal at 222 nm. This wavelength reflects pH-dependent changes in the regular secondary structure of the protein N- and C-terminal helices (*31*). CD spectra were recorded at room temperature with a PiStar-180 spectrometer (Applied Photophysics, Leatherhead, Surrey, United Kingdom) installed at the Macromolecular Interactions Facility (University of North Carolina, Chapel Hill, NC). A 50 mM stock solution of freshly IMTSL-labeled protein was prepared and kept on ice between the measurements. In a typical experiment, an aliquot from the stock solution was diluted with freshly prepared buffer solutions of the required pH to the final protein concentration of ca. 6−8 μM.

EPR Measurements. X-Band (9.5 GHz) EPR measurements were carried out at room temperature with a Varian (Palo Alto, CA) Century Series E-109 spectrometer. Typically, aqueous solutions were drawn into polytetrafluoroethylene (PTFE) capillaries (0.81 mm × 1.12 mm, NewAge Industries, Inc., Southampton, PA), and the capillaries were folded twice and inserted into standard 3 mm × 4 mm quartz EPR tubes. Rigid-limit EPR spectra were recorded in the aqueous buffer/20% glycerol mixture with a finger dewar (Wilmad-Labglass, Buena, NJ) filled with liquid nitrogen (77 K).

The W-band (94 GHz) EPR spectrometer has been described previously (*32, 33*). The magnetic field sweep up to ±550 G from the main field was provided by a water-cooled coaxial sweep coil. The feedback circuit was based on a Danfysik Ultrastab 860R current transducer (GMW Associates, Redwood City, CA) that provided a linearity better than 5 ppm and a resolution of 0.05 ppm. Because the transducer operates on a zero-flux principle, it allowed

us to avoid a problem of temperature stabilization at high currents. Measured resettability was better than 100 μA (out of a ±15.4 A maximum), and the stability was better than 10 ppm of the maximum scan width. This scanning coil provided magnetic field scanning in steps as fine as 30 mG.

The scan and the center of the magnetic field were calibrated with a Metrolab precision NMR teslameter PT 2025 (GMW Associates). The microwave frequency was measured with a source-locking microwave counter (model 578, EIP Microwave Inc., San Jose, CA). The cavity was a cylindrical-type TE_{01n} cavity ($n = 2$ or 3 depending upon tuning) with an unloaded quality factor of ca. 4000.

Typically, for W-band EPR spectroscopy, liquid samples were drawn into thin-wall, clear-fused quartz capillaries (purchased from VitroCom, Inc., Mountain Lakes, NJ) by capillary action. The diameter of the capillaries was varied depending on the solvent. The smallest capillaries, 0.20 mm × 0.33 mm in diameter, were used for polar aqueous samples, while for nonpolar solvents such as toluene, the size of the capillaries was 0.70 mm × 0.87 mm. After the capillaries had been filled with solutions, both ends of the capillaries were sealed with a Critoseal (Fisher Scientific, Pittsburgh, PA) in a way that the seals were always outside the EPR resonator. The typical volume of aqueous samples inside the W-band EPR cavity was less than 150−200 nL.

Special care was taken to ensure accurate and repeatable *g*-factor measurements. A few days before the experiments, the main superconductive coil was parked within 10 G of the target magnetic field. Typically, the magnetic field drift was stabilized within the first 6 h. After this stabilization, the center field of the magnet and magnetic field scan range of the water-cooled coil were calibrated with a Metrolab NMR teslameter. Magnetic field scans of the same width were used for both calibrations and experiments. To simplify the calibration procedure in experiments with nitroxide radicals, we have used a 100 μM aqueous solution of PDT for cross calibration of the magnetic field. The measurements of A_{iso} from independently calibrated scans at X- and W-bands were found to be consistent and equal to 16.01 ± 0.01 G, while a g_{iso} of 2.00550(6) was determined from W-band EPR measurements. By acquiring Tempone spectra before and after the experiments, we have found that the magnetic field was stable and that *g* factors were repeatable to 1 ppm. The drift of the main superconductive coil was determined to be less than 0.1 ppm/h.

RESULTS AND DISCUSSION

EPR Calibration of IMTSL and IMTSL-Labeled Thiols. Initial characterization of IMTSL was carried out using X-band EPR. For aqueous solutions of IMTSL, single-component fast-motion EPR spectra were observed over a pH range from 0.1 to 6.5 units. When the pH was increased from 0.1 to 3.0, the isotropic nitrogen hyperfine splitting (A_{iso}) increased from 14.34 ± 0.05 to 15.75 ± 0.03 G. The change in A_{iso} was found to be reversible and is known to be associated with the N3 atom protonation (*34*).

The effect of pH on the nitroxide EPR spectra is associated with proton exchange between a radical R• and its conjugated acid R•H$^+$:

$$R^{\bullet} + BH^+ \rightleftarrows R^{\bullet}H^+ + B \qquad (1)$$

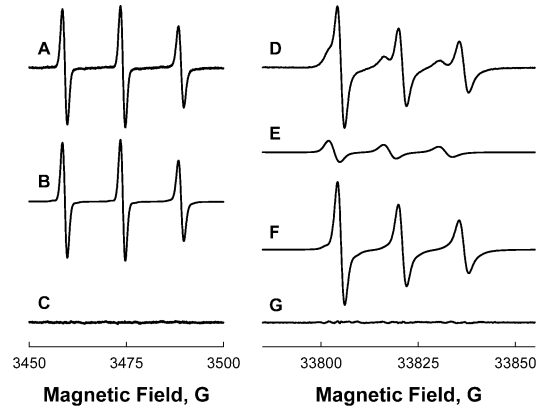

FIGURE 1: (A) Experimental room-temperature X-band (9.5 GHz) EPR spectrum of IMTSL taken at pH 2.06. (B) Least-squares simulated spectrum of the nitroxide at pH 2.06. (C) Residual of the fit, the difference between the experimental spectrum and the best-fit spectrum. (D) Experimental room-temperature W-band (95 GHz) EPR spectrum of IMTSL taken at pH 2.1. (E and F) Best-fit components for protonated and nonprotonated forms of IMTSL, respectively. (G) Residual of the fit.

Previously, Khramtsov and co-workers considered conditions for fast and slow proton exchange between the R• and R•H$^+$ forms of pH-sensitive nitroxides (*28*). Assuming that for IMTSL this reaction is diffusion-controlled with a rate constant k_1 of $\approx 10^{10}$ M^{-1} s^{-1} and that the difference in the resonant frequencies of the high-field nitroxide components at X-band does not exceed a $\Delta\upsilon$ of 4×10^6 s^{-1} (i.e., 1.4 G), then the EPR spectra are in a fast exchange if (*28*)

$$pK_a < \log(k_1/\Delta\nu) \approx 3.4 \qquad (2)$$

This estimate is in agreement with fast-exchange EPR spectra observed for IMTSL at X-band for all the pH values studied.

Figure 1A shows an example of an experimental IMTSL X-band EPR spectrum taken at pH 2.06. At this intermediate pH, the radical is expected to exist as a mixture of protonated and nonprotonated forms. The spectrum was least-squares simulated using a fast-exchange model and software we described earlier (Figure 1B) (*35, 36*). The residual of the fit, a difference between the experimental and the best-fit spectrum (Figure 1C), shows that the model of a single nitroxide component fits the data exceptionally well. Thus, at this pH, chemical exchange between the R• and R•H$^+$ species is fast on the X-band EPR time scale.

Figure 2 (●) shows A_{iso} values of IMTSL as a function of pH as determined from least-squares simulations of fast-exchange X-band EPR spectra. The overall A_{iso} titration curve fits well to the Henderson−Hasselbalch equation:

$$A_{iso} = \frac{A_a \times 10^{pH-pK_a} + A_b}{1 + 10^{pH-pK_a}} \qquad (3)$$

where A_a and A_b are the isotropic nitrogen hyperfine coupling constants for the acidic form and the basic form of IMTSL, respectively. The best-fit results are shown as a solid line in Figure 2 and are also summarized in Table 1. The difference between A_a and A_b for IMTSL (ΔA_{iso}) was found to be 1.39 ± 0.06 G, which is similar to that of the "parent" radical 2,2,3,4,5,5-hexamethylimidazolidine 1-oxyl, RH3 [$\Delta A_{iso} \approx$ 1.3 G (*26, 37*)] and is one of the largest ΔA_{iso} values among the nitroxides of the imidazolidine series (*26*).

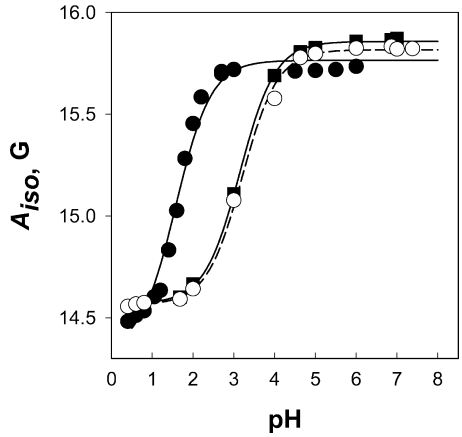

FIGURE 2: Weighted average A_{iso} values determined from least-squares simulations of fast-exchange X-band EPR spectra as a function of pH: (●) IMTSL, (○) IMTSL-cys, and (■) IMTSL-glu. Corresponding least-squares Henderson−Hasselbalch titration curves are shown as solid (IMTSL and IMTSL-glu) and dashed (IMTSL-cys) lines.

Table 1: Titration Parameters of Free IMTSL and with Thiols Attached As Determined from Least-Squares Fitting of Room-Temperature X-Band (9.5 GHz) EPR Data to the Henderson−Hasselbalch Equation [a]

	A_{iso}(acid)	A_{iso}(base)	pK_a
IMTSL	14.34 ± 0.05	15.75 ± 0.03	1.58 ± 0.03
IMTSL-cys	14.56 ± 0.02	15.82 ± 0.02	3.21 ± 0.04
IMTSL-glu	14.57 ± 0.02	15.86 ± 0.03	3.15 ± 0.03
IMTSL-iso-1-cytochrome *c*	14.46 ± 0.03	15.81 ± 0.05	1.78 ± 0.07

[a] Isotropic *g* factors were not measured because of the insufficient accuracy of X-band data.

It was observed that above neutral pH IMTSL would rapidly form biradicals which became evident from characteristic five-line EPR spectra (not shown). These species were not characterized for pH dependence. Biradicals have also been observed for MTSL under similar conditions. One could expect that at basic pH, some of the labels' methanethiosulfonate groups are hydrolyzed to thiols, which would then react with the remaining methanethiosulfonates forming disulfide biradicals.

It is well established that upon proton-exchange reactions both the nitrogen hyperfine coupling constant *A* and *g* factor of nitroxides are affected; however, at X-band the line shifts, ΔB, due to Δg_{iso} are smaller than those originating from ΔA_{iso}, or the line width, and therefore are typically not resolved (*28, 34, 37*). Specifically, for IMTSL the difference in g_{iso} between R$^{\bullet}$ and R$^{\bullet}$H^{+}species (Δg_{iso}) is $\approx 2.8 \times 10^{-4}$, which translates into a ΔB of ≈0.47 G at X-band (9.5 GHz), smaller than the line width of 1−1.2 G. With a 10-fold increase in resonance field/frequency achieved at W-band (95 GHz), ΔB is increased to ≈4.7 G, exceeding both the field-independent change in ΔA_{iso} (≈1.4 G) and the line width of 2 G. This leads to a significantly improved spectral resolution. Figure 1D illustrates this on an example of an IMTSL W-band EPR spectrum that shows a partially resolved protonated and nonprotonated nitroxide species at an intermediate pH of 2.1, while the X-band spectrum measured at essentially the same pH (2.06) (Figure 1A) does not. The two-component IMTSL W-band EPR spectra are indicative of a slow chemical-exchange regime on the W-band EPR time scale.

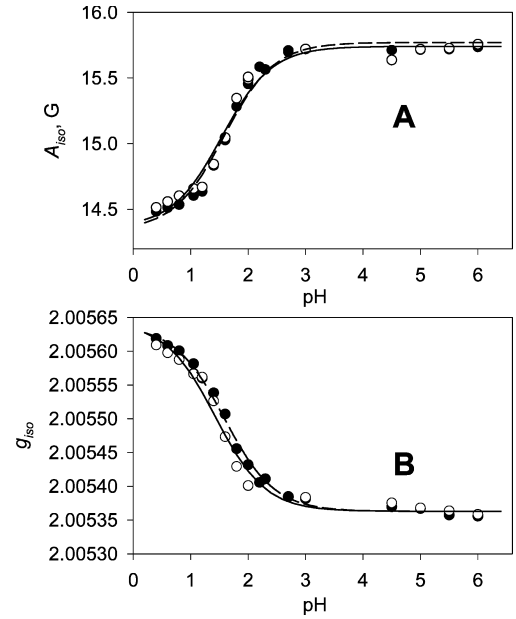

FIGURE 3: Titration data for A_{iso} (A, top) and g_{iso} (B, bottom) obtained from fitting of W-band EPR spectra of IMTSL recorded at 19 (●) and 37 °C (○). Corresponding least-squares fits to the Henderson−Hasselbalch equation are shown as dashed and solid lines, respectively.

At intermediate pH values, the W-band EPR spectra of IMTSL, such as those shown in Figure 1D, were modeled as a superposition of two nitroxide species, the parameters of which were adjusted during the Levenberg−Marquardt optimization. Spectra E and F of Figure 1 show the best-fit components for protonated and nonprotonated forms of IMTSL, respectively. A residual of the fit (Figure 1G) demonstrates that this approximate model fits the experimental spectrum (Figure 1D) rather well. From such a fitting, g_{iso}, A_{iso}, line widths, and double integrals of the individual components, f_1 and f_2, were determined. To compare the results of one- and two-component fitting (such as W- and X-band titration curves), it is more convenient to plot a weighted sum of, for example, $A_{iso} = (f_1A_{1,iso} + f_2A_{2,iso})/(f_1 + f_2)$ as a function of pH rather than just the fraction of the individual component. Figure 3 shows titration data for both g_{iso} and A_{iso} obtained from fitting of 19 °C W-band EPR spectra (●). Corresponding least-squares Henderson−Hasselbalch titration curves are shown as dashed lines, and the best-fit titration parameters are listed in Table 2 along with the standard deviations predicted from such a fitting.

Comparison of A_{iso}(acid), A_{iso}(base), and pK_a for IMTSL obtained from X-band (Table 1) and W-band (Table 2) experiments at 19 °C demonstrates essentially the same results being obtained in these two experiments. Thus, the very similar accuracy of pK_a determination for free tumbling pH-sensitive nitroxides could be achieved regardless of the microwave frequency of EPR experiments or the regime of the spin exchange: fast at X-band and slow at W-band. Notably, W-band measurements allow one to monitor pK_a from *g*-factor changes: pK_a(g_{iso}) of 1.59 ± 0.03 identical to that derived from A_{iso} [pK_a(A_{iso}) = 1.58 ± 0.03]. The importance of *g*-factor measurements for local pK_a determination of larger macromolecules will be discussed in the following sections of this report.

To examine whether the pK_a of IMTSL is affected by moderate changes in temperature during EPR experiments,

Table 2: Titration Parameters of Free IMTSL (at 19 and 37 °C) and with Thiols Attached (at 19 °C) As Determined from Least-Squares Fitting of W-Band (94 GHz) EPR Data to the Henderson−Hasselbalch Equation

	A_{iso}(acid)	A_{iso}(base)	pK_a (A_{iso})	g_{iso}(base)	g_{iso}(acid)	pK_a (g_{iso})
IMTSL, 19 °C	14.34 ± 0.04	15.75 ± 0.03	1.58 ± 0.03	(2.005363 ± 3) × 10^{-6}	(2.005638 ± 5) × 10^{-6}	1.59 ± 0.03
IMTSL, 37 °C	14.36 ± 0.06	15.75 ± 0.04	1.54 ± 0.08	(2.005363 ± 6) × 10^{-6}	(2.005643 ± 13) × 10^{-6}	1.42 ± 0.07
IMTSL-cys	14.52 ± 0.04	15.79 ± 0.04	3.29 ± 0.08	(2.005356 ± 5) × 10^{-6}	(2.005613 ± 5) × 10^{-6}	3.29 ± 0.08
IMTSL-glu	14.51 ± 0.01	15.82 ± 0.02	3.17 ± 0.03	(2.005353 ± 2) × 10^{-6}	(2.005620 ± 4) × 10^{-6}	3.12 ± 0.04
CP	16.01 ± 0.04	16.20 ± 0.04	4.03 ± 0.08	(2.005315 ± 2) × 10^{-6}	(2.005349 ± 2) × 10^{-6}	4.18 ± 0.07

g_{iso} and A_{iso} titration curves were also measured at 37 °C using W-band EPR [Figure 3 (○), corresponding least-squares fits to the Henderson−Hasselbalch equation are shown as solid lines]. Titration parameters are given in Table 2. It is clear that the W-band data at 37 °C follow closely the results at 19 °C. This indicates a relatively small enthalpy of the IMTSL proton-exchange reaction and is in accord with literature data for other compounds (*38*). However, the 37 °C data show somewhat larger scatter which is evident from larger standard deviations predicted from the fit (Table 2). The likely reason for the scatter is that with an increase in temperature, the rate of proton exchange increases and the spectra start to approach an intermediate regime for which neither one- nor two-site simple models are fully applicable.

It is well established that chemical modifications of nitroxide side chains close to N3 would affect the pK_a of the imidazolidine nitroxides (*26*). Thus, to utilize IMTSL in SDSL EPR studies, the label has to be calibrated when it is attached to cysteine-containing molecules, such as amino acids and/or small peptides. To assess these changes, two additional W-band EPR titration calibration experiments, one with the label attached to a cysteine (IMTSL-cys) and the other with IMTSL-labeled glutathione (IMTSL-glu), were carried out. Similar to those of free IMTSL, the EPR spectra of these compounds taken at 19 °C and intermediate pH values were indicative of a slow exchange at W-band and fast exchange at X-band. Both IMTSL-cys and IMTSL-glu EPR titration experiments were carried out up to pH 9.0. The disulfide bond formed in these adducts is sufficiently stable under these alkaline conditions, which was ascertained from the reversible character of the titration curves. All spectra were least-squares simulated as described above. For clarity and to avoid overlapping data points, the W-band titration curves for IMTSL-cys and IMTSL-glu (Figure 4) are plotted separately from the free IMTSL data (Figure 3) while X-band titration data are shown in the same graph (Figure 2). The least-squares parameters of the Henderson−Hasselbalch fits are given in Tables 1 and 2.

Several observations could be made from the EPR titration data given in Tables 1 and 2. First, for each of the two IMTSL thiol adducts studied, EPR titration parameters derived from either X- and W-band spectra were found to be the same, demonstrating that the same accuracy could be achieved regardless of the spin-exchange regime. Second and most notably, the pK_a values of these two adducts were shifted to a more basic pK_a of 3.21 ± 0.04 for IMTSL-cys and 3.15 ± 0.03 for IMTSL-glu (X-band measurements) from the pK_a of the free label (1.58 ± 0.03 units). Also, A_{iso}(acid) for IMTSL−thiol adducts was somewhat larger than that of free IMTSL, while the increase in A_{iso}(base) was comparable with the experimental error.

EPR titration parameters in Tables 1 and 2 indicate that the main effect of replacing MTS with the disulfide group, as a result of the reaction with thiols, is the change in the pK_a of the tertiary amino group rather than in isotropic A_{iso} and g_{iso} for both basic and acidic forms of the nitroxide. This is expected because the N3 protonation site is only three chemical bonds away from the site of modification, while the EPR-reporting nitroxide moiety is distanced by five chemical bonds. In nitroxide radicals, the electronic spin density is chiefly localized on the π orbital of the NO fragment and the modification of the side chain away from that fragment is not expected to cause any significant electron redistribution. Therefore, A_{iso} and g_{iso} for both basic and acidic nitroxide forms are not affected by the side chain modification. However, the pK_a of the protonatable tertiary amino group that is positioned closer to the side chain becomes affected: reaction with a thiol converts the methanethiosulfonate group into a less electronegative disulfide side chain, thus shifting the pK_a of the formed adduct to more basic values.

In principle, the presence and the ionization state of other groups in the side chain could also affect the nitroxide EPR spectra. Such groups could be found in both IMTSL adducts. For example, the carboxylic and amino functionalities of IMTSL-cys are expected to exhibit pK_a values that are close to those of cysteine (respective pK_a values are 1.71 and 8.33) and cystine (pK_a values are 1.0 and 2.1 for two carboxylic groups and 8.02 and 8.71 for two amino groups, respectively) (*39*). However, for IMTSL-cys, no measurable changes in either A_{iso} or g_{iso} were observed at these pH values: both

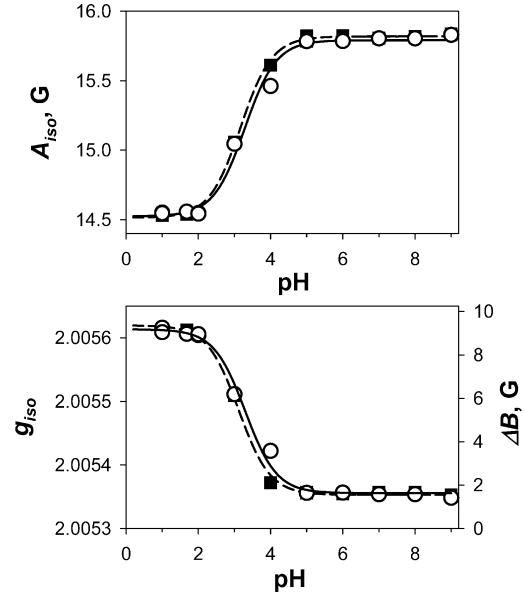

FIGURE 4: Experimental titration data for g_{iso} (bottom panel) and A_{iso} (top panel) obtained from fitting of W-band EPR spectra of IMTSL-cys (○) and IMTSL-glu (■). The corresponding least-squares Henderson−Hasselbalch titration curves are shown as solid and dashed lines, respectively.

EPR parameters followed the single-transition Henderson−Hasselbalch titration curves. The same result was observed for the IMTSL-glu adduct, the side chain of which contains groups with pK_a values that could be close to those of a glutamine (pK_{a1} = 2.2; pK_{a2} = 9.1) and to the carboxylic group of the glycine moiety of the tripeptide itself (pK_a = 3.59) (*40*). The absence of any measurable effects of the ionizable side chain groups on EPR titration parameters is in line with the fast decay of inductive electronic effects along the chain of σ-bonds; any through-space electric field effects on either the nitroxide moiety or the pK_a of the tertiary amino group are expected to be small. Thus, when attached to thiols, IMTSL reports on the local pH experienced by the N3 amino group. The pK_a of this group is found to be unaffected by other ionizable groups present in the side chain, at least when this chain is short and interchain interactions and tertiary structure are absent as in these small unstructured peptides. However, one could expect that for more complex macromolecules, the presence of tertiary interactions and local folds would affect the electrostatic environment of the probe, resulting in measurable changes in pK_a reported by the label.

Labeling of Model Proteins with IMTSL. Comparison of the chemical structure of IMTSL in its basic form to that of MTSL indicates many similarities that raise expectations for essentially the same EPR parameters. Moreover, similar physical properties, including solubility and the same structure of the attachment group, make MTSL labeling protocols applicable for site-directed protein chain modification with IMTSL. Uncharged IMTSL is expected to affect the protein structure in essentially the same way as MTSL does: the latter label has been shown to have small, if any, effects on the protein structure and function which was demonstrated by scanning 30 different cysteine mutants of T4 lysozyme (*25*). Moreover, on the basis of the similarity of molecular sizes and geometry of nitroxide rings of MTSL and the basic form of IMTSL and the same length and the structure of the attachment tether, one would expect very similar rotational dynamics for the two spin-labels and, therefore, similar EPR spectra.

To illustrate these similarities, we have closely followed the MTSL protocol to label the single native cysteine 102 (C102) of iso-1-cytochrome *c* with IMTSL (*41*). Figure S1 (Supporting Information) shows that the shapes of far-UV CD spectra of the native protein (C102) and the one labeled with IMTSL (C102-IMTSL) are essentially identical, confirming the absence of nitroxide perturbation effects on the content of the α-helical structure (*31*).

Room-temperature X-band EPR spectra of iso-1-cytochrome *c* labeled with MTSL and IMTSL are shown in Figure 5. The spectrum of IMTSL-labeled iso-1-cytochrome *c*, taken at pH 6.6 (Figure 5B), is very similar to that of MTSL-labeled iso-1-cytochrome *c* (Figure 5A), demonstrating that for this site the nanosecond-scale rotational dynamics of the nitroxide and, thus, the interactions of the spin-label with the protein backbone are unaffected by the presence of an uncharged amine group in the imidazolidine ring. The isotropic nitrogen hyperfine coupling constant (A_{iso}) for MTSL-labeled iso-1-cytochrome *c* is 16.13 ± 0.05 G which is within the experimental error of the A_{iso} observed for this spin-label in water (16.09 ± 0.03 G). For IMTSL-labeled iso-1-cytochrome *c*, the A_{iso} of 15.81 ± 0.05 G is the same as the A_{iso} of 15.82 ± 0.02 G observed for IMTSL-cys in the basic form (Table 1). This comparison of isotropic nitrogen hyperfine coupling constants indicates that the nitroxide moieties of both spin-labeled side chains are fully exposed to the aqueous phase.

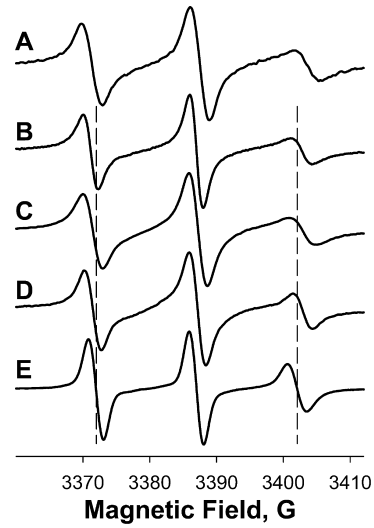

FIGURE 5: Representative room-temperature X-band EPR spectra of iso-1-cytochrome *c* labeled at the unique Cys102 with MTSL (A) recorded in 10 mM MOPS buffer at pH 6.6 and IMTSL (B−E) recorded in 50 mM buffers at various pH values: (B) 6.6, (C) 5.0, (D) 3.0, and (E) 1.68. Vertical dashed lines correspond to approximate positions of the zero cross points of the nitrogen hyperfine coupling components of the IMTSL-labeled iso-1-cytochrome *c* spectrum measured at pH 1.68.

To demonstrate the utility of IMTSL for monitoring local protein electrostatics, we have carried out EPR titration of spin-labeled iso-1-cytochrome *c*. Figure 5 shows a series of X-band EPR spectra of this protein in the pH range from 6.6 to 1.68. For all pH values, the label tethered at C102, the penultimate C-terminal amino acid residue located in the loop region, experienced only small rotational restrictions as indicated by EPR spectra characteristic for the fast motion regime. This is typical for surface-exposed protein side chains (*42*). One could also expect that such a progressive lowering of pH would trigger denaturing of this protein. Indeed, far-UV CD of IMTSL-labeled iso-1-cytochrome *c* in the pH range from 7.03 to 1.68 measured at 208 and 222 nm indicated a gradually decreased content of the α-helical fold (Figure S2, Supporting Information). Specifically, CD spectra taken in the range from pH 7.03 to 3.99 revealed the presence of a native-like but reduced α-helical signature. The α-helical content drastically decreased when the pH dropped from 3.99 to 3.54, and the protein was completely denatured at pH <2.99. These CD data are in a good agreement with spin-labeling EPR data that show the progressive disappearance of the residual slow/intermediate motion spectral components at pH ≤3.0 (Figure 5). Thus, the local environment of this spin-label attached to the protein loop becomes more disordered as the protein unfolds.

Lowering the pH value also resulted in a decrease in the apparent isotropic nitrogen hyperfine coupling constant (A_{iso}) of IMTSL-labeled iso-1-cytochrome *c* measured as a distance between the low field and the central nitrogen hyperfine EPR components. The A_{iso} versus bulk pH titration plot [Figure 6 (○)] yielded a pK_a of 1.78 ± 0.07 that was largely different from that of unstructured IMTSL-cys (pK_a = 3.21 ± 0.04).

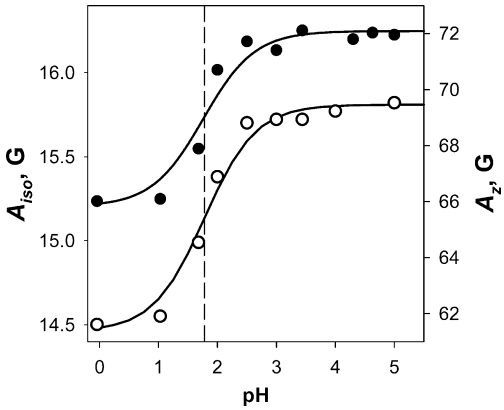

FIGURE 6: Experimental X-band EPR titration data for IMTSL-labeled iso-1-cytochrome *c* measured at room temperature from changes of isotropic nitrogen hyperfine coupling constant, A_{iso} (○, left axis), and from an anisotropic hyperfine component A_z (●, right axis) defined as the splitting between the outer peaks of rigid limit EPR spectra measured at 77 K. Solid lines show the least-squares Henderson−Hasselbalch titration curves that yielded nearly identical pK_a values: 1.78 ± 0.07 for the A_{iso} plot and 1.76 ± 0.10 for A_z. Dashed line defines an average pK_a of 1.77.

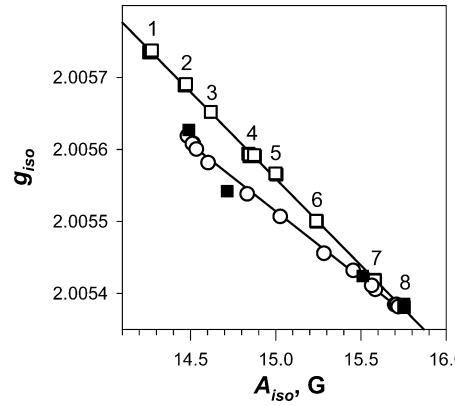

FIGURE 7: Isotropic magnetic parameters g_{iso} vs A_{iso} obtained from solution W-band EPR spectra. (□) IMTSL in a series of protic and aprotic solvents and their mixtures: (1) toluene, (2) acetonitrile, (3) acetone, (4) 2-propanol, (5) ethanol, (6) water/ethanol solution (3:7, v/v), (7) water/ethanol solution (7:3, v/v), and (8) water (buffered to pH 6.0). Titration parameters for IMTSL (○) and IMTSL-P11 (■). Linear regressions are shown as solid lines and discussed in the text.

This difference is attributed to the local electrostatic environment of the label that remains present even after the protein unfolds. It should be noted here that protonation of the spin probe itself is not the reason for the protein denaturing: according to the CD data, it occurs between pH ≈4.0 and ≈3.0 which is well above the pK_a of 1.78 ± 0.07 determined for IMTSL-labeled iso-1-cytochrome *c* by EPR.

IMTSL-labeled iso-1-cytochrome *c* X-band titration experiments performed under the rigid-limit EPR conditions (77 K) produced a pK_a essentially the same as that for room temperature [Figure 6 (●)]. This result indicates that the local electrostatic environment of this spin-labeled protein side chain is unaffected by freezing the protein solution at 77 K. Representative rigid-limit EPR spectra of IMTSL-labeled iso-1-cytochrome *c* are shown in Figure S3 of the Supporting Information.

Differentiating Effects of Local Polarity and Proton Exchange: g_{iso}−A_{iso} Correlation Plots. In applications of pH-sensitive nitroxides to studies of local electrostatics of proteins and membranes from changes in magnetic parameters of the radical, one should also consider factors other than proton-exchange reactions for potential contributions. Some of the most important of such factors are the solvent dielectric constant and hydrogen bonding. To investigate these solvent effects, we have carried out a calibration of g_{iso} and A_{iso} of IMTSL for a series of protic and aprotic solvents, including water, water/ethanol mixtures, several alcohols, acetone, acetonitrile, and toluene. Figure 7 (□) shows a correlation plot for g_{iso} versus A_{iso} obtained from fitting room-temperature W-band EPR spectra. The estimated errors are within the size of the symbols. The data shown in Figure 7 strongly suggest the existence of a linear correlation. Previously, Kawamura and co-workers reported that for another nitroxide, di-*tert*-butyl nitroxide (DTBN), g_{iso} versus A_{iso} plots have two different linear correlations for protic and aprotic solvents (*16*). Recent W-band measurements of isotropic magnetic parameters of another nitroxide, Tempo, strongly suggested that g_{iso} is proportional to A_{iso} regardless whether the solvent is protic (*43*).

While this paper is not intended for development of a detailed theoretical understanding of the observed linear correlation, a qualitative explanation could be built on the basis of the existing theories. Indeed, it is well established that both g_{iso} and A_{iso} are approximately proportional to the spin density at the nitrogen atom (*44–47*) while the electronic *g* factor has some additional dependence on the excitation energy of the oxygen lone-pair orbital, which is affected by the solvent dielectric constant and hydrogen bonding (*48*). If a hydrogen bond donor molecule would be approaching the oxygen atom only at certain defined angles that are asymmetric with respect to the N−O bond, then one would expect anisotropic effects on the *g* factor and, likely, some different correlations between g_{iso} and A_{iso} for hydrogen bonding versus non-hydrogen bonding solvents. However, for random rapid collisions that are typical for solutions studied here at room temperature, one cannot expect any asymmetry in the formation of transient hydrogen bonds with respect to the nitroxide N−O axis. Thus, the main effect of the collisions with the protic molecules would be on the spin density at the oxygen atom, the same as for aprotic molecules. It is worthwhile to note here that fast spin exchange between nitroxides in different local environments would not affect this linear correlation, and the same empirical plot could be used to assign effective "polarity" in the vicinity of the nitroxide, as demonstrated for a nitroxide partitioned in two compartments of a phospholipid bilayer interdigitated at high ethanol concentrations (*43*).

One interesting question is whether the same correlation between g_{iso} and A_{iso} would hold for the protonated form of IMTSL. Figure 7 demonstrates that the correlations are different. Empty circles show that with a decrease in pH, weighted parameters A_{iso} and g_{iso} clearly fall below the linear correlation plot for the IMTSL in the nonprotonated form. This deviation is related to the effect of an asymmetric charge, located chiefly on N3, on the spin density at the oxygen atom. As one would expect, the protonated form of IMTSL would have a somewhat different electronic configuration of the nitroxide moiety that cannot be mimicked by symmetric rearrangement of the solvent molecules with respect to the axis of the N−O bond. Then, g_{iso}(base) and

A_{iso}(base) for the nonprotonated form of the IMTSL in various solvents should fall onto one straight line, while g_{iso}(acid) and A_{iso}(acid) would belong to another one. It is also easy to see that as long as both g_{iso} and A_{iso} report on the same proton-exchange reaction (and follow the same Henderson−Hasselbalch equation), the plot of weighted g_{iso} versus A_{iso} upon protonation [Figure 7 (○)] would also follow a straight line but with a different slope. Such linear correlations (solid lines in Figure 7) could be used for differentiating polarity and proton-exchange effects on IMTSL isotropic magnetic parameters. It is worthwhile to note here that while the A_{iso} of 14.34 ± 0.05 G for the acidic form of IMTSL is very close to the A_{iso} of 14.47 ± 0.05 G observed for the basic form of this nitroxide in acetonitrile, the difference in isotropic g factors between these two species (Δg_{iso}) is (5.1 ± 0.7) × 10^{-5}. While at X-band this Δg_{iso} translates into an only ca. 85 mG line shift, which is hard to measure, at W-band this difference amplifies to a measurable 850 mG. Thus, the high g-factor resolution achieved by W-band EPR is essential for assigning whether changes in magnetic parameters of IMTSL are caused by proton exchange or just by local polarity effects.

The deviation of g_{iso} from the g_{iso}−A_{iso} polarity correlation plot as shown in Figure 7 is still rather small when compared with the overall change in g_{iso} in the course of the proton-exchange reaction: Δg_{iso} = (5.1 ± 0.7) × 10^{-5} and (27.5 ± 0.7) × 10^{-5}, respectively. This is because the primary effect of the electrical charge localized at N3 is on the spin density at the oxygen atom of the nitroxide moiety and the effect on the oxygen lone-pair orbital contributes as a smaller correction. This also means that for reliable differentiation of polarity and pH effects it is desirable to have a nitroxide with large changes in g_{iso} and A_{iso} upon protonation.

To illustrate the latter, we have carried out W-band EPR titration and solvent polarity calibration experiments for another nitroxide, 3-carboxy-2,2,5,5-tetramethylpyrrolidine 1-oxyl (CP). Results of these titrations are summarized in panels A and B of Figure 8 and listed in Table 2. The data are in general agreement with the previously published 220 GHz EPR results of Gulla and Budil, who utilized this nitroxide for studies of effects of the electric field on the nitroxide **g** matrix (*37*). For this spin probe, the changes in g_{iso} and A_{iso} upon proton-exchange reaction are small when compared with those reported here for IMTSL or with another imidazolidine nitroxide RH3 (*37*). The main reasons for smaller Δg_{iso} and ΔA_{iso} values observed for CP are (i) a longer distance between the charged carboxylic group and nitroxide moiety and therefore smaller effective electric field when compared with that of either IMTSL or RH3 and (ii) a compensating effect of polar solvent molecules surrounding the carboxylic group (*37*). In addition, for CP the electric charge is expected to be delocalized in a greater degree than for IMTSL. On the basis of these two factors, small Δg_{iso} and ΔA_{iso} and a larger charge delocalization, one could expect that for CP, g_{iso} should be approximately proportional to A_{iso} regardless of the ionization state of the carboxyl group. Indeed, Figure 8C demonstrates that for this nitroxide, all the isotropic magnetic parameters measured in solvents of different polarities and also in aqueous buffers from pH 1.0 to 10.0 [Figure 8 (○)] follow the same linear dependence regardless of the charge of the carboxylic

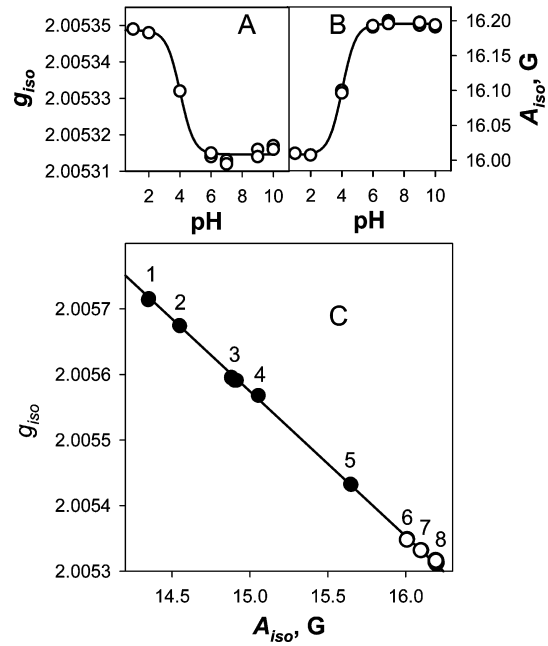

FIGURE 8: Room-temperature W-band EPR g_{iso} (A) and A_{iso} (B) titration experiments and solvent polarity calibration experiments (C) for 3-carboxy-2,2,5,5-tetramethylpyrrolidine 1-oxyl (CP). The top panels show experimental titration data for g_{iso} (A) and A_{iso} (B) with the corresponding least-squares Henderson−Hasselbalch titration curves shown as solid lines with the best-fit parameters listed in Table 2. Panel C shows a combined g_{iso} vs A_{iso} correlation plot: (1) toluene, (2) acetonitrile, (3) acetone, (4) 2-propanol, (5) ethanol, (6) water/ethanol solution (3:7, v/v), (7) water/ethanol solution (7:3, v/v), and (8) water, buffered to pH 6.0. Titration data from panels A and B are shown as empty circles in front of the filled circles corresponding to water and water/ethanol mixture data.

group or whether the solvent is protic or aprotic. Thus, for this nitroxide, polarity and titration effects cannot be differentiated which was illustrated for IMTSL (at least at magnetic fields of W-band EPR). It is also worthwhile to note here that CP is yet another example of a nitroxide with the same linear correlation between g_{iso} and A_{iso} for protic and aprotic solvents.

Measurements of Local pK_a Values of a P11 Peptide Fragment of Glycoprotein Laminin B1 Chain. To illustrate the utility of IMTSL in site-directed pK_a measurements and the use of our HF EPR method for differentiating pH and polarity effects, we have labeled a synthetic P11 peptide, a fragment of the laminin B1 chain (Cys-Asp-Pro-Gly-Tyr-Ile-Gly-Ser-Arg), with IMTSL at the single cysteine. This peptide was found to reduce the degree of colonization of lung cells with malignant melanoma by >90%, when administered together with the melanoma cells by injection into mice via the tail vein (*49*). Iwamoto et al. speculated that this peptide could inhibit lung tumor colony formation by blocking tumor cell invasion through basement membranes (*49*).

As a first step in understanding the role of electrostatics in interaction of this peptide with membranes, we have carried out room-temperature EPR titration experiments. Figure 9 shows representative X- and W-band EPR spectra from ca. 0.3 mM IMTSL-P11 in a 50 mM phosphate buffer at pH 6.0. At both EPR frequencies, the spectra fall into the fast motional regime as demonstrated by least-squares simulation of the W-band spectrum (Figure 9B−D). For this

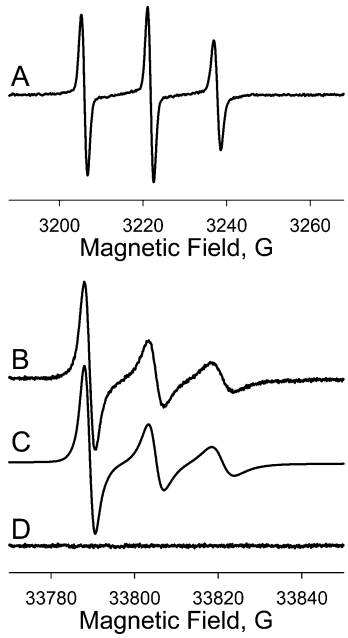

FIGURE 9: Representative room-temperature fast-motion X-band (A) and W-band (B) EPR spectra from ca. 0.3 mM IMTSL-P11 in a 50 mM phosphate buffer at pH 6.0.; (C) Least-squares simulation of the W-band spectrum (B). (D) Fit residual, a difference between the experimental spectrum and the simulated spectrum.

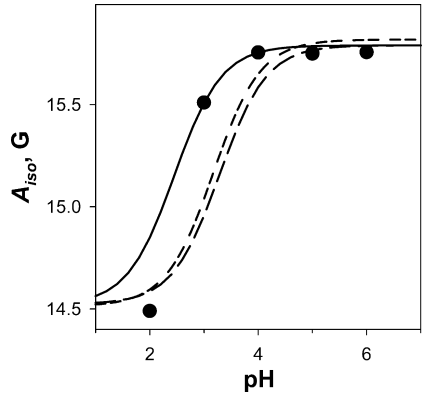

FIGURE 10: Experimental titration data for A_{iso} obtained from simulation of W-band EPR spectra of IMTSL-P11 (●). The least-squares Henderson−Hasselbalch titration curves for IMTSL-glu and IMTSL-cys (short- and long-dashed lines, respectively) are shown for comparison.

spectrum, the isotropic nitrogen hyperfine coupling constant (A_{iso}) of 15.75 ± 0.01 was essentially the same as A_{iso}(base) for IMTSL-cys and IMTSL-glu (Table 2), indicating that the nitroxide is fully exposed to the aqueous phase.

With a decrease in pH, the W-band EPR spectrum of IMTSL-P11 was split into two components (not shown) similar to that of IMTSL-cys and IMTSL-glu. While at pH 4.0 and 3.0 the effective A_{iso} was decreased only slightly, at pH 2.0 A_{iso}(acid) was essentially the same as for other IMTSL-modified thiols (see Figure 10 and Table 1). Since one could expect some conformational changes to occur for a peptide at an acidic pH, only the data from pH 3.0 to 6.0 were fitted to the Henderson−Hasselbalch equation. Moreover, because all the data presented here for IMTSL and its adducts with thiol-containing molecules indicate that the A_{iso}(base) and A_{iso}(acid) values are approximately unaffected by the side chain substitutions, the latter values were fixed during the optimization and only the pK_a was varied. The results of the fit are shown in Figure 10 as a solid line together with the least-squares Henderson−Hasselbalch curves for IMTSL-glu and IMTSL-cys (short- and long-dashed lines, respectively). Figure 10 demonstrates that the pK_a of IMTSL-P11 (2.5 ± 0.1) is lower than that of either IMTSL-glu or IMTSL-cys (p$K_a \approx 3.18$). Unfortunately, the titration curve for IMTSL-P11 cannot be completed at low pH because the EPR signal from IMTSL-P11 rapidly decayed even at pH 2 and no EPR signals were observed at pH <2.

One could argue that the observed changes in A_{iso} could be related to a decrease in an effective local polarity arising from peptide conformational changes rather than the reversible protonation of the spin-label. For example, the tyrosine residue could approach the nitroxide ring, thus decreasing local polarity and, as a result, lowering A_{iso}. To discriminate between these two scenarios, we have compared g_{iso} and A_{iso} at each pH value with the g_{iso}−A_{iso} correlation plot. Figure 7 shows that isotropic magnetic parameters for IMTSL-P11 (■) closely follow the IMTSL pH titration correlation plot but not the polarity plot. Thus, the observed changes in g_{iso} and A_{iso} are related to the proton-exchange reaction of the nitroxide label but not the local polarity changes.

As discussed above, we have experimentally shown that the pK_a values of IMTSL-glu and IMTSL-cys are not affected by the ionization state of the functional groups in the side chain. However, larger peptides, such as P11, could adopt a folded or a partially folded state through tertiary interactions. Specifically for P11, the energy-optimized structure (Figure S4, Supporting Information) shows that the nitroxide ring attached to a cysteine could be placed in the proximity of the carboxylic group of the aspartic acid. Previously, it has been shown that in proteins the pK_a of the carboxylic group in an aspartic acid residue could vary from 2.0 to 4.93 (*50, 51*). However, for IMTSL-P11, the shift of the titration curve to a more acidic region as compared with that for IMTSL-cys and IMTSL-glu could not be explained by the effect of the aspartic acid. The negatively charged carboxylate should stabilize the protonated form of the proximal imidazolidine moiety, shifting its apparent pK_a to a more basic pH region. Another possible reason for the shift in the pK_a to the acidic region could be destabilization of the protonated form of the nitroxide by an effective positive charge, which was acquired by a globular peptide structure as the result of protonation of other basic groups (e.g., guanidine moiety of Arg).

To summarize, we have synthesized a new pH-sensitive thiol-specific imidazolidine nitroxide label methanethiosulfonic acid *S*-(1-oxyl-2,2,3,5,5-pentamethylimidazolidin-4-ylmethyl) ester (IMTSL) and characterized this nitroxide in its free form and covalently tethered to a cysteine, short peptides (glutathione and P11 peptide), and the native cysteine 102 of iso-1-cytochrome *c* from *S. cerevisiae*. It was shown that EPR titration experiments could be carried out at W-band by measuring the effect of protonation on either A_{iso} or g_{iso}, as each magnetic parameter responds to an asymmetric charge acquired upon protonation and located chiefly on N3. To differentiate reversible protonation and solvent effects on magnetic parameters of IMTSL, g_{iso} and A_{iso} were also measured for a series of protic and aprotic solvents. It was found that for IMTSL, g_{iso} correlates linearly with A_{iso}, but the correlations are different for the neutral and charged forms of the nitroxide. This finding was attributed to effects of solvent on the spin density at the

oxygen atom of the NO group and on the excitation energy of the oxygen lone-pair orbital. It is proposed to employ g_{iso} versus A_{iso} correlation plots for differentiating polarity and protonation effects in spin labeling experiments. The utility of such an approach has been demonstrated with an example of a synthetic P11 peptide. IMTSL was also employed for labeling of the unique cysteine of iso-1-cytochrome *c*. EPR spectra of this protein labeled with IMTSL were found to be very similar to that labeled with MTSL, and CD data revealed no perturbations to the overall protein structure. Titration curves deduced from either room-temperature or rigid-limit IMTSL EPR spectra yielded nearly identical pK_a values, demonstrating that both approaches are equally applicable. Notably, the protonation of the spin probe itself is not the reason for the protein denaturing as the latter, according to the CD data, occurred at a pH higher than the pK_a of the spin-labeled side chain.

This study shows that pH-sensitive nitroxides in combination with enhanced spectral resolution of high-field EPR spectroscopy could considerably extend the range of biophysical experiments carried out with site-directed spin labeling techniques. While this work was being prepared, a report by Möbius and co-workers on probing local pH within the proton channel of bacteriorhodopsin light-driven proton pump from *Halobacterium salinarium* by means of multi-frequency EPR of IMTSL has been published (*52*). One of the conclusions in that paper was that high-field EPR in combination with pH-sensitive spin-labels opens a new avenue for investigating protein systems. The latter finding further reaffirmed conclusions of our study regarding IMTSL being an essential tool for mapping the complex landscape of proteins' electrostatics.

ACKNOWLEDGMENT

We are grateful to Prof. T. I. Smirnova (North Carolina State University) for numerous suggestions and fruitful discussions.

SUPPORTING INFORMATION AVAILABLE

Far-UV CD spectra of native and IMTSL-labeled iso-1-cytochrome *c*, results of CD experiments on pH-induced denaturation of IMTSL-labeled iso-1-cytochrome *c*, selected rigid-limit X-band EPR spectra of IMTSL-labeled iso-1-cytochrome *c*, and energy-minimized structure of P11. This material is available free of charge via the Internet at http://pubs.acs.org.

REFERENCES

1. Yang, A.-S., Gunner, M. R., Sampogna, R., Sharp, K., and Honig, B. (1993) On the calculation of pK_a's in proteins. *Proteins 15*, 252–265.
2. Gilson, M. K. (1993) Multiple-site titration and molecular modeling: Two rapid methods for computing energies and forces for ionizable groups in proteins. *Proteins 15*, 266–282.
3. Honig, B., and Nicholls, A. (1995) Classical electrostatics in biology and chemistry. *Science 268*, 1144–1149.
4. Sheinerman, F. B., Norel, R., and Honig, B. (2000) Electrostatic aspects of protein-protein interactions. *Curr. Opin. Struct. Biol. 10*, 153–159.
5. Halgren, T. A., and Damm, W. (2001) Polarizable force fields. *Curr. Opin. Struct. Biol. 11*, 236–242.
6. Simonson, T. (2001) Macromolecular electrostatics: Continuum models and their growing pains. *Curr. Opin. Struct. Biol. 11*, 243–252.
7. Pitera, J. W., Falta, M., and van Gunsteren, W. F. (2001) Dielectric properties of proteins from simulation: The effects of solvent, ligands, pH, and temperature. *Biophys. J. 80*, 2546–2555.
8. Ko, J., Murga, L. F., André, P., Yang, H., Ondrechen, M. J., Williams, R. J., Agunwamba, A., and Budil, D. E. (2005) Statistical criteria for the identification of protein active sites using theoretical microscopic titration curves. *Proteins 59*, 183–195.
9. Ondrechen, M. J., Clifton, J. G., and Ringe, D. (2001) THEMATICS: A simple computational predictor of enzyme function from structure. *Proc. Natl. Acad. Sci. U.S.A. 98*, 12473–12478.
10. Ko, J., Murga, L. F., Wei, Y., and Ondrechen, M. J. (2005) Prediction of active sites for protein structures from computed chemical properties. *Bioinformatics 21* (Suppl. 1), i258–i265.
11. Sharp, K. A., and Brooks, C. L. (2001) Old wine in new bottles? *Curr. Opin. Struct. Biol. 11*, 209–211.
12. Tollinger, M., Forman-Kay, J. D., and Kay, L. E. (2002) Measurement of side-chain carboxyl pK_a values of glutamate and aspartate residues in an unfolded protein by multinuclear NMR spectroscopy. *J. Am. Chem. Soc. 124*, 5714–5717.
13. Luptak, A., Ferre-DrAmare, A. R., Zhou, K., Zilm, K. W., and Doudna, J. A. (2001) Direct pK_a Measurement of the Active-Site Cytosine in a Genomic Hepatitis Delta Virus Ribozyme. *J. Am. Chem. Soc. 123*, 8447–8452.
14. Teng, C.-L., and Bryant, R. G. (2006) Spin relaxation measurements of electrostatic bias in intermolecular exploration. *J. Magn. Reson. 179*, 199–205.
15. Cohen, B. E., McAnaney, T. B., Park, E. S., Jan, Y. N., Boxer, S. G., and Jan, L. Y. (2002) Probing protein electrostatics with a synthetic fluorescent amino acid. *Science 296*, 1700–1703.
16. Kawamura, T., Matsunami, S., and Yonezawa, T. (1967) Solvent effects on the *g*-value of di-*t*-butyl nitric oxide. *Bull. Chem. Soc. Jpn. 40*, 1111–1115.
17. Griffith, O. H., Dehlinger, P. J., and Van, S. P. (1974) Shape of the hydrophobic barrier of phospholipid bilayers (Evidence for water penetration in biological membranes). *J. Membr. Biol. 15*, 159–192.
18. Ondar, M. A., Grinberg, O. Ya., Dubinskii, A. A., and Lebedev, Ya. S. (1985) Study of the effect of the medium on the magnetic-resonance parameters of nitroxyl radicals by high-resolution EPR spectroscopy. *Sov. J. Chem. Phys. 3*, 781–792.
19. Smirnova, T. I., Chadwick, T. G., Voinov, M. A., Poluektov, O., van Tol, J., Ozarowski, A., Schaaf, G., Ryan, M. M., and Bankaitis, V. A. (2007) Local Polarity and Hydrogen Bonding Inside the Sec14p Phospholipid-Binding Cavity: High-Field Multi-Frequency Electron Paramagnetic Resonance Studies. *Biophys. J. 92*, 3686–3695.
20. Smirnova, T. I., Chadwick, T. G., MacArthur, R., Poluektov, O., Song, L., Ryan, M. M., Schaaf, G., and Bankaitis, V. A. (2006) The Chemistry of Phospholipid Binding by the *Saccharomyces cerevisiae* Phosphatidylinositol Transfer Protein Sec14p as Determined by Electron Paramagnetic Resonance Spectroscopy. *J. Biol. Chem. 281* (46), 34897–34908.
21. Steinhoff, H.-J., Savitsky, A., Wegener, C., Pfeiffer, M., Plato, M., and Möbius, K. (2000) High-field EPR studies of the structure and conformational changes of site-directed spin labeled bacteriorhodopsin. *Biochim. Biophys. Acta 1457*, 253–262.
22. Wegener, C., Savitsky, A., Pfeiffer, M., Möbius, K., and Steinhoff, H.-J. (2001) High-field EPR-detected shifts of magnetic tensor components of spin label side chains reveal protein conformational changes: The proton entrance channel of bacteriorhodopsin. *Appl. Magn. Reson. 21*, 441–452.
23. Hubbell, W. L., and Altenbach, C. (1994) Site-Directed Spin Labeling of Membrane Proteins, in *Membrane Protein Structure: Experimental Approaches* (White, S. H., Ed.) pp 224−248, Oxford University Press, London.
24. Feix, J. B., and Klug, C. S. (1998) Site-Directed Spin Labeling of Membrane Proteins and Peptide-Membrane Interactions, in *Biological Magnetic Resonance, Spin Labeling: The Next Millennium* (Berliner, L. J., Ed.) Vol. 14, pp 251−282, Plenum Press, New York.
25. Mchaourab, H. S., Lietsow, M. A., Hideg, K., and Hubbell, W. L. (1996) Motion of spin-labeled side chains in T4 lysozyme. Correlation with protein structure and dynamics. *Biochemistry 35*, 7692–7704.
26. Khramtsov, V. V., and Volodarsky, L. B. (1998) Use of Imidazoline Nitroxides in Studies of Chemical Reactions: ESR Measurements of the Concentration and Reactivity of Protons, Thiols, and Nitric Oxide, in *Biological Magnetic Resonance, Spin Labeling: The Next*

Millennium (Berliner, L. J., Ed.) Vol. 14, pp 109−180, Plenum Press, New York.
27. Khramtsov, V. V., Marsh, D., Weiner, L., and Reznikov, V. A. (1992) The application of pH-sensitive spin labels to studies of surface potential and polarity of phospholipid membranes and proteins. *Biochim. Biophys. Acta 1104*, 317–324.
28. Khramtsov, V. V., Weiner, L. M., Eremenko, S. I., Belchenko, O. I., Schastnev, P. V., Grigor'ev, A. I., and Reznikov, V. A. (1985) Proton exchange in stable nitroxyl radicals of the imidazoline and imidazolidine series. *J. Magn. Reson. 61*, 397–408.
29. Smirnov, A. I., Ruuge, A., Reznikov, V. A., Voinov, M. A., and Grigor'ev, I. A. (2004) Site-directed electrostatic measurements with a thiol-specific pH-sensitive nitroxide: Differentiating local pK_a and polarity effects by High-Field EPR. *J. Am. Chem. Soc. 126*, 8872–8873.
30. Weast, R. C., and Astle, M. J., Eds. (1980) *CRC Handbook of Chemistry and Physics*, p D-149, CRC Press, Inc., Boca Raton, FL.
31. Myer, Y. P. (1985) Circular Dichroism Studies of Electron-Transport Components, in *Current Topics in Bioenergetics*, Vol. 14, pp 149−188, Academic Press, Inc., New York.
32. Wang, W., Belford, R. L., Clarkson, R. B., Davis, P. H., Forrer, J., Nilges, M. J., Timken, M. D., Watczak, T., Thurnauer, M. C., Norris, J. R., Morris, A. L., and Zwang, Y. (1994) Very high-frequency EPR: 94 GHz instrument and applications to primary reaction centers from photosynthetic red bacteria and to other disordered systems. *Appl. Magn. Reson. 6*, 195–215.
33. Nilges, M. J., Smirnov, A. I., Clarkson, R. B., and Belford, R. L. (1999) Electron paramagnetic resonance W-band spectrometer with a low-noise amplifier. *Appl. Magn. Reson. 16*, 167–183.
34. Khramtsov, V. V., Weiner, L. M., Grigoriev, I. A., and Volodarsky, L. B. (1982) Proton exchange in stable nitroxyl radicals. EPR study of the pH of aqueous solutions. *Phys. Chem. Lett. 91*, 69–72.
35. Smirnov, A. I., and Belford, R. L. (1995) Rapid quantitation from inhomogeneously broadened EPR spectra by a Fast Convolution Algorithm. *J. Magn. Reson., Ser. A 113*, 65–73.
36. Smirnova, T. I., Smirnov, A. I., Clarkson, R. B., and Belford, R. L. (1995) W-band (95 GHz) EPR spectroscopy of nitroxide radicals with complex proton hyperfine structures: Fast motion. *J. Phys. Chem. 99*, 9008–9016.
37. Gulla, A. F., and Budil, D. E. (2001) Orientation dependence of electric field effects on the *g* factor of nitroxides measured by 220 GHz EPR. *J. Phys. Chem. B 105*, 8056–8063.
38. Olofsson, G., and Hepler, L. G. (1975) Thermodynamics of ionization of water over wide ranges of temperature and pressure. *J. Solution Chem. 4*, 127–143.
39. Ralph, T. R., Hitchman, M. L., Millington, J. P., and Walsh, F. C. (1994) The electrochemistry of L-cystine and L-cysteine: Part 1: Thermodynamic and kinetic studies. *J. Electroanal. Chem. 375*, 1–15.
40. Povse, V. G., and Olabe, J. A. (1998) Kinetics and mechanism of ligand interchange in the [Ru^{III}(edta)L] complexes; L = cysteine and related thiolates. *Transition Met. Chem. 23*, 657–662.
41. Qu, K., Vaughn, J. L., Sienkiewicz, A., Scholes, C. P., and Fetrow, J. S. (1997) Kinetics and Motional Dynamics of Spin-Labeled Yeast *Iso*-1-cytochrome *c*: 1. Stopped-Flow Electron Paramagnetic Resonance as a Probe for Protein Folding/Unfolding of the C-Terminal Helix Spin-Labeled at Cysteine 102. *Biochemistry 36*, 2884–2897.
42. Pyka, J., Osyczka, A., Turyna, B., Blicharski, W., and Froncisz, W. (1999) Probing *iso*-1-cytochrome *c* structure by site-directed spin labeling and electron paramagnetic resonance techniques. *Acta Biochim. Pol. 46* (4), 889–899.
43. Smirnov, A. I., and Smirnova, T. I. (2001) Resolving Domains of Interdigitated Phospholipid Membranes with 95 GHz Spin Labeling EPR. *Appl. Magn. Reson. 21*, 453–467.
44. Mukerjee, P., Ramachandran, C., and Pyter, R. A. (1982) Solvent effects on the visible spectra of nitroxides and relation to nitrogen hyperfine splitting constants. Nonempirical polarity scales for aprotic and hydroxylic solvents. *J. Phys. Chem. 86*, 3189–3197.
45. Burghaus, O., Plato, M., Rohrer, M., Möbius, K., MacMillan, F., and Lubitz, W. (1993) 3-mm High-field EPR on semiquinone radical anions $Q^{\bullet-}$ related to photosynthesis and on the primary donor $P^{\bullet+}$ and acceptor $Q_A^{\bullet-}$ in reaction centers of *Rhodobacter sphaeroides* R-26. *J. Phys. Chem. 97*, 7639–7647.
46. Ondar, M. A., Grinberg, O. Y., Dubinskii, A. B., Shestakov, A. F., and Lebedev, Y. S. (1983) EPR spectroscopy in 2-mm range and magnetic-resonance parameters. *Khim. Fiz. 2*, 54–60.
47. Ondar, M. A., Grinberg, O. Y., Dubinskii, A. B., and Lebedev, Y. S. (1984) Study of the effect of the medium on the magnetic-resonance parameters of nitroxyl radicals by high-resolution electron-paramagnetic-res spectroscopy. *Khim. Fiz. 3*, 527–536.
48. Stone, A. J. (1963) Gauge invariance of the *g* tensor. *Proc. R. Soc. London, Ser. A 271*, 424–434.
49. Iwamoto, Y., Robey, F. A., Graf, J., Sasaki, M., Kleinman, H. K., Yamada, Y., and Martin, G. R. (1987) YIGSR, a synthetic laminin pentapeptide, inhibits experimental metastasis formation. *Science 238* (4830), 1132–1134.
50. Noble, M. A., Gul, S., Verma, C. S., and Brocklehurst, K. (2000) Ionization characteristics and chemical influences of aspartic acid residue 158 of papain and caricain determined by structure-related kinetic and computational techniques: Multiple electrostatic modulators of active-centre chemistry. *Biochem. J. 351*, 723–733.
51. Lohse, D. L., Denu, J. M., Santoro, N., and Dixon, J. E. (1997) Roles of aspartic acid-181 and serine-222 in intermediate formation and hydrolysis of the mammalian protein-tyrosine-phosphatase PTP1. *Biochemistry 36*, 4568–4575.
52. Möbius, K., Savitsky, A., Wegener, C., Plato, M., Fuchs, M., Schnegg, A., Dubinskii, A. A., Grishin, Y. A., Grigor'ev, I. A., Kühn, M., Duché, D., Zimmermann, H., and Steinhoff, H.-J. (2005) Combining high-field EPR with site-directed spin labeling reveals unique information on proteins in action. *Magn. Reson. Chem. 43*, S4–S19.

BI800272F